Performance of a volatiles distributor equipped with internal baffles under different fluidization regimes

Powder Technology 409 (2022) 117807

Contents lists available at ScienceDirect

Powder Technology

journal homepage: www.journals.elsevier.com/powder-technology

Performance of a volatiles distributor equipped with internal baffles under different fluidization regimes

Xiaoyun Li *, Anders Lyngfelt, Carl Linderholm, Bo Leckner, Tobias Mattisson

Department of Space, Earth and Environment, Chalmers University of Technology, Hörsalsvägen 7b, 412 96 Gothenburg, Sweden

HIGHLIGHTS

- The volatiles distributor (VD) was further developed by equipping internal baffles.
- The horizontal distribution of volatiles is improved significantly by the VD.
- The slip of volatiles from the bottom can be reduced by the internal baffles.

GRAPHICAL ABSTRACT

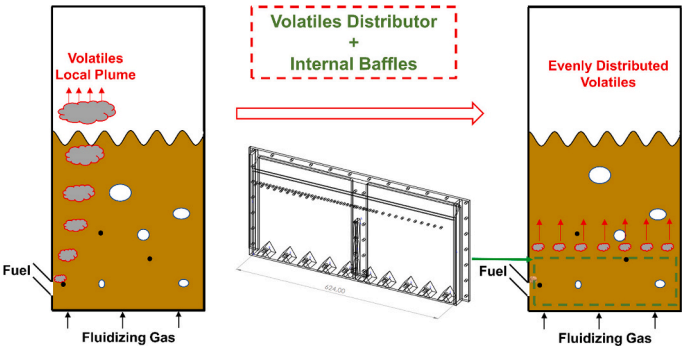

ARTICLE INFO

Keywords:
Chemical looping combustion
Biomass
Fuel reactor
Volatiles distributor
Internal baffles
Gas-solid contacting
CO_2 reduction
Cold-flow model

ABSTRACT

Chemical looping combustion of biomass is a promising carbon capture technology due to its inherent CO_2 separation advantage. However, complete fuel conversion, particularly volatiles conversion for biomass, is usually not achieved in the fuel reactor. A novel concept named volatiles distributor (VD) has been proposed and tested in a cold-flow fluidized-bed, which shows good potential to achieve a more uniform horizontal distribution of the volatiles and improve the gas-solid contact. In this work, the VD has been further developed by introducing an array of internal baffles inside the VD. The objective is to improve the horizontal gas distribution and reduce the volatiles slip from the bottom of the VD. The results show that the uniformity of the horizontal distribution is improved significantly by the VD equipped with the internal baffles, especially in the single and multiple bubble regimes. The volatiles slip from the bottom of the VD is reduced by the installation of internal baffles according to the visual observation, even though there is a higher CO_2 concentration detected above the bottom edge of the VD near the wall. A pronounced back-mixing of gas near the wall in the main riser may be the principal reason for the higher measured CO_2 concentration.

1. Introduction

The climate change target to limit the global average temperature increase to well below 2 °C above pre-industrial levels before 2100 can only be achieved by a deep reduction in CO_2 and other greenhouse gas emissions in the coming decades [1]. Bio-Energy with Carbon Capture

* Corresponding author.
E-mail address: xiaoyun.li@chalmers.se (X. Li).

https://doi.org/10.1016/j.powtec.2022.117807
Received 5 April 2022; Received in revised form 28 June 2022; Accepted 31 July 2022
Available online 2 August 2022

and Storage (BECCS) as a negative CO_2 emission technology is promising to fulfill the emission reduction target. Chemical looping combustion of biomass (Bio-CLC) could play an important role for CO_2 capture, as this technology enables the production of a pure stream of CO_2 inherently in the process. As shown in Fig. 1, biomass absorbs CO_2 in the air through photosynthesis and can be utilized by chemical looping combustion (CLC) to produce energy. CO_2 in air is captured by combining photosynthesis from renewable biomass and CLC, and stored geologically to achieve negative CO_2 emissions [2].

The CLC process includes two interconnected fluidized-bed reactors, i.e. air reactor and fuel reactor as shown in Fig. 1. Oxygen carriers (OC) are circulated between these two reactors in order to transfer oxygen from the air to the fuel and avoid the direct contact between them. The OC take oxygen from air in the air reactor and the oxidized OC provide oxygen for the fuel in the fuel reactor in a N_2-free environment. Therefore, after the condensation of steam in the flue gas of the fuel reactor, pure CO_2 is produced, and the energy penalty required for CO_2 separation from N_2 in conventional combustion is prevented.

Biomass goes through several steps in the fuel reactor. Drying and devolatilization may take place in a matter of seconds after the injection of the fuel [3,4]. Upon devolatilization, char and a large volume of volatiles are formed since biomass has larger content of volatiles compared to coal and other similar fuels. The volatiles can react with OC directly to produce CO_2 and H_2O. The reaction between the char and the OC are not direct but involves an intermediate gasification step where char reacts with H_2O to form CO and H_2. The whole process of biomass conversion is shown in Fig. 2.

Both bubbling and circulating fluidized beds are widely used for the design of the fuel reactor [5–8]. Bubbling fluidized beds are operated at lower superficial fluidization velocity. However, the produced combustibles may bypass the dense bed as bubbles and there are fewer solids in the freeboard, which cause less gas-solid contacting time in the fuel reactor. Circulating fluidized beds are operated at higher superficial fluidization velocity and give more homogenous solids distribution over the height of the reactor, which can result in longer gas-solid contacting time, less amount of OC and less operation cost. However, it might require more fan power. The pressure drop over the gas distributor between the wind box and the dense bed is not only related to the fan energy consumption but also the fluidization regime, i.e. single bubble regime and multiple bubble regime, in the fuel reactor [9,10]. Both the configurations of the fuel reactor and the fluidization regimes are crucial for the gas-solid contacting and gas conversion in the fuel reactor.

The common practice in fluidized-bed boilers is to feed the fuel above the dense bottom zone. In CLC, however, it is desired that gases from the fuel are released as far down in the bed as possible to achieve good contact between volatiles and OC. Hence, solid fuel in-bed feed or feed at the loop-seal connecting to the fuel reactor is favorable. The volatiles released rapidly from the solid fuel in the dense bed, in particular for the high-volatile fuel biomass, may also have an influence on the gas-solid contacting regime in the fuel reactor. Lyngfelt and Leckner [11] designed a 1000 MW_{th} CLC unit and described the change of gas velocity in the fuel reactor over the height as presented in Fig. 3. The bottom gas, either steam or a combination of steam and recycled CO_2 is mainly used to keep the bed fluidized. There are two major gas flows at the bottom of the fuel reactor originating from the char gasification and the volatiles. The syngas produced by gasification will appear in the dense phase and make the dense phase 'self-fluidizing', which is likely to change the bottom bed to a turbulent regime, bring more OC to the freeboard and be helpful for improving the gas-solid contacting.

Ideally, biomass should be completely converted into CO_2 and H_2O in the fuel reactor. However, there are three possible deviations from the ideal bio-CLC process due to the limited fuel residence time and non-sufficient gas-solid contact in the fuel reactor [11]. These deviations, i.e. incomplete gas conversion, char loss to the air reactor, and elutriated char in the flue gas, are shown in Fig. 4. They are quantified by three performance indicators, i.e. oxygen demand, carbon capture efficiency, and solid fuel conversion.

The performance could be improved in two ways, either by the mechanical and chemical properties of OC or by the design and operation of the reactors.

More than 70 different OC have been tested in actual operation of CLC pilots, of which more than 3000 h are with solid fuels [12]. Some ores and waste materials have reasonable cost and show reactive potential [13–15]. Some synthetic materials have shown higher potential to improve the fuel conversion in the fuel reactor [16–18]. The materials with oxygen uncoupling capability (CLOU materials) can release gaseous oxygen in the fuel reactor and improve the solid fuel conversion significantly [19,20]. Full fuel conversion has been achieved by using copper or copper manganese mixed oxides [21,22]. However, a trade-off should be made between the reactivity and the lifetime or cost of the OC due to the loss of oxygen OC with the ash leaving the system.

Different designs and modifications of the fuel reactor have been

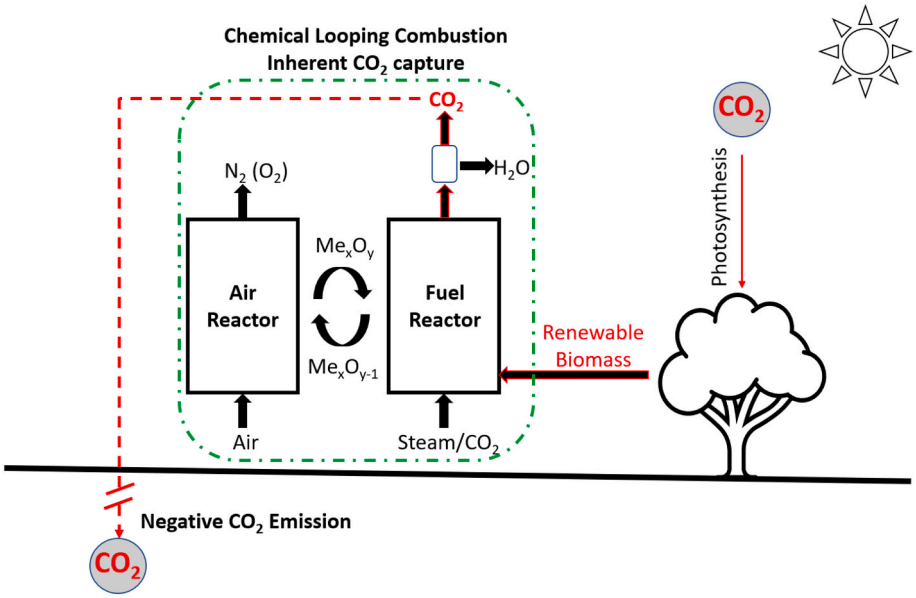

Fig. 1. Negative CO_2 emission and power generation achieved by bio-CLC.

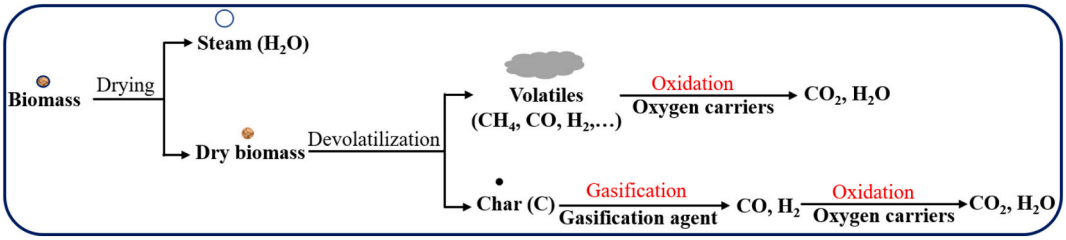

Fig. 2. Biomass reactions in the fuel reactor of CLC.

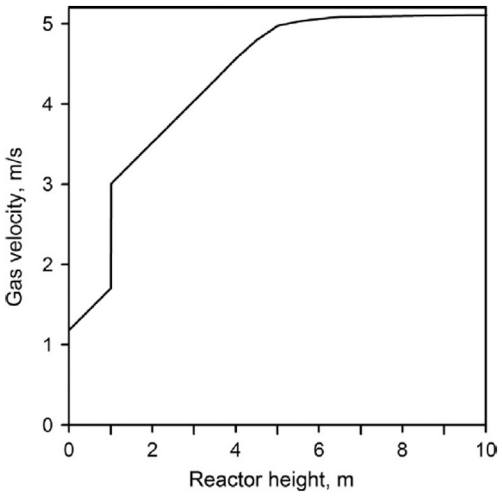

Fig. 3. Gas velocity in fuel reactor versus height.

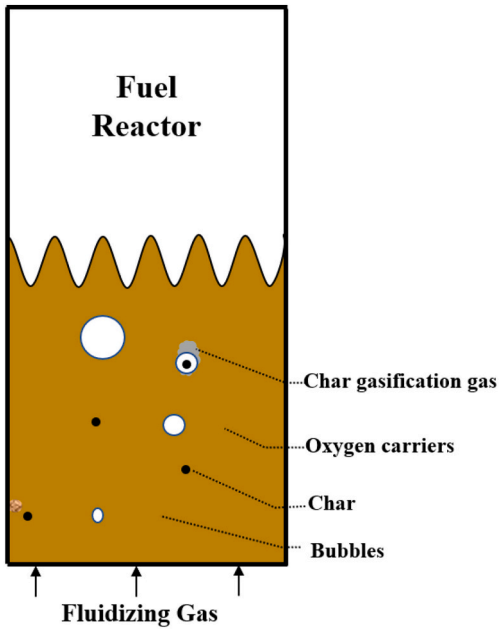

Fig. 4. Inadequate performance of the fuel reactor. [11].

proposed aiming for higher solid fuel conversion. The concept of carbon stripper was proposed in order to reduce the char slip from the fuel reactor and to increase the residence time of char in fuel reactor. It has been tested with fossil-derived fuels in different scales of small CLC pilot units, which show improved carbon capture efficiency [5,23–25]. Due to the more reactive and smaller content of char in biomass, pilot operation with biomass in a CLC unit without carbon stripper has demonstrated that it is possible to improve the carbon capture efficiency to more than 98% [26]. A two-stage fuel reactor was proposed and proved to have better combustion performance compared to previous CLC facilities [27]. Guío-Pérez et al. [28] investigated the influence of ring-type internals equipped inside the fuel reactor, which showed a positive effect on the solids residence time at least in a laboratory-scale unit. Pérez-Vega et al. [29] modified the fuel reactor of 50 kW_{th} unit by the ring-type internals with the objective of improving the solids distribution and enhancing the gas-solid contact. An improved oxidation of volatiles in the form of CH_4 and full conversion of H_2 were achieved by this modification.

Li et al. [9] proposed and investigated a novel concept named volatiles distributor (VD) in a cold-flow fluidized-bed model aiming at more even horizontal distribution of the volatiles and improved gas-solid contact in the fuel reactor. The VD improved the horizontal distribution of volatiles, especially when the fluidization velocity was high. However, a potential bottom leakage of gas from the VD was identified, which means the volatiles may slip away below the lower edge of the distributor, and thus, negatively impact the uniformity of the horizontal gas distribution.

Internals in fluidized beds, i.e. baffles, tubes, packings and inserted bodies, can be used to limit the bubble size, adjust the entrainment of particles, change the hydrodynamic characteristics and improve the gas-solid reaction [30]. The main features of baffles are to break bubbles and enhance the gas-solid mixing and contacting by redistributing the bubbles in the radial direction [31–33]. The bottom leakage of the VD used in the previous work was estimated to be caused by the pressure fluctuations due to the big bubbles [9]. Hence, the baffles could be a solution for this bottom leakage issue, since it can prevent continuous growth of the bubbles to some extent and reduce the fluctuations in bed surface inside the VD associated with bed material moving in and out of the VD.

The objective of this work is to design internal baffles and to assess the effect of such baffles inside the VD on the performance of a VD including the uniformity of the horizontal distribution and the volatiles slip under different fluidization regimes.

2. Experimental system

2.1. Cold flow model configuration

The cold-flow fluidized-bed model includes a wind box, a riser and a cyclone. The riser has a length × width × height of 700 mm×120 mm×8500 mm. The front side of the riser is made from Perspex glass, which allows visual observation of fluidization inside the VD. The VD is installed at the bottom of the riser at a height of 114 mm, i.e. from the bottom of the VD to the bottom of the riser. The fluidization air is provided by fans. The volatiles are simulated by the air from the fans and by pure CO_2 as a tracer gas. There is an injection hole for simulated volatiles at the front plate, which allows the simulated volatiles to flow into the VD, cf. Fig. 5.

Along the height of the riser, there are twenty-four taps for pressure measurements, which are installed in the middle of the backside of the riser. The pressure measurement in the wind box is located at the right side, shown as a pink point in the right top corner of the wind box in

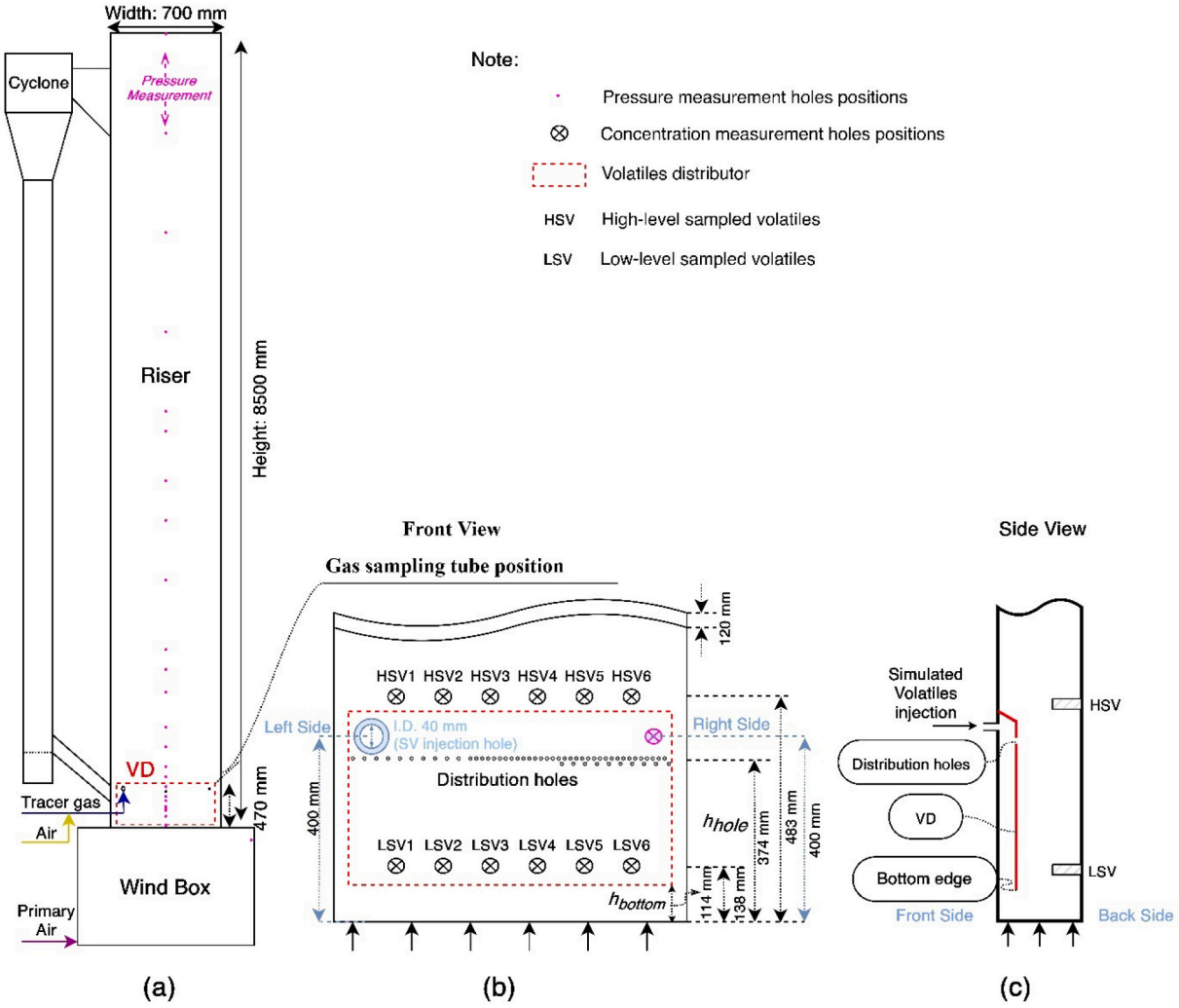

Fig. 5. (a) Cold-flow circulating fluidized-bed model equipped with the VD and pressure and CO_2 concentration measurement systems; (b) Front view of the riser bottom, the distribution holes are seen in detail in Fig. 7; (c) Side view, the side view is shown in further detail in Fig. 9.

Fig. 5 (a). There are two more pressure taps to measure the pressure drop between the inside and outside of the VD, one of which is at the middle of backside of the riser with the same height of the distribution holes, i.e. 374 mm. The other is for the pressure measurement inside the VD, which is to the right top corner of the front plate, i.e. the pink crossed circle shown in the gas sampling tube position of Fig. 5 (b).

There are thirteen gas sampling tubes in the experimental system, which are the higher-level ones (HSV1-HSV6), the lower-level ones (LSV1-LSV6) and the one for sampling the gas inside the VD. The latter is located in the top right corner of the front plate, shown as a pink crossed circle shown in Fig. 5 (b). The gas sampled from the tubes after the filters, flows through the pump and the gas analyzer in the following sequence: LSV6, LSV5, LSV4, LSV3, LSV2, LSV1, HSV6, HSV5, HSV4, HSV3, HSV2, HSV1 and finally the top right corner of the VD. The flowrate is 1 L_n/min. For each measurement position, the gas flows into the gas analyzer for 210 s in total, the first 90 s are for stabilization and the remaining 120 s are for recording data to calculate the average concentration.

2.2. Volatiles distributor equipped with internal baffles

The basic concept of the VD is to use channels or arms that are open downwards. These arms are immersed close to the bottom of a fluidized bed and have distribution holes on both sides. If no volatiles are added, part of the fluidizing gas would go upwards into the box and be flowing out through the distribution holes. The bed surface inside the box would then be at the level of the distribution holes. The arms are connected to an otherwise closed freeboard where the fuel is added onto a part of the fluidized bed. As the volatiles are released they will follow the channels and flow out through the distribution holes. The bed surface inside the box would be lowered because of the pressure drop caused by the volatiles flow through the holes. A more detailed design theory of the VD has been introduced in a previous work [9].

The performance of the VD has been investigated under different operational conditions and configurations of distribution holes in the previous work [9,10], which shows the effectiveness of the VD on the uniformity of the horizontal distribution of volatiles at the bottom of the riser. The sketch of the VD is presented in Fig. 6. The detailed information about the configuration of the distribution holes is shown in Fig. 7. There are fewer distribution holes on the side closest to the volatiles injection port (cf. Fig. 5), and more holes to the right side, which is further away from the volatiles injection side. All the distribution holes have a diameter of 5 mm. This arrangement of distribution holes, i.e. uneven distribution of the holes, improves the uniformity of the horizontal gas distribution accomplished by the VD according to previous work by the authors [10]. Therefore, this configuration is applied to this work as well.

The internal baffles, which are designed to improve the performance of the VD, are arranged at the bottom of the VD, shown in Fig. 6. The internal baffle was designed based on the hourglass concept in order to

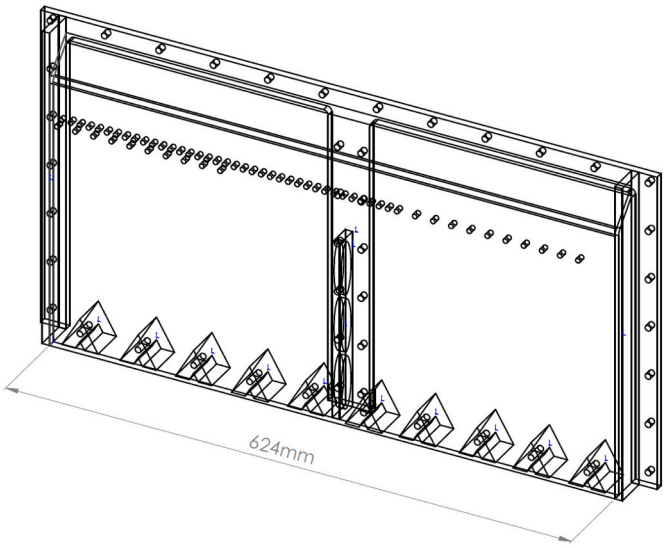

Fig. 6. Internal baffles arrangement inside the VD (mounted on the front plate of the riser at bottom).

slow down the solids descent velocity and mitigate the surface fluctuations of the bed inside the VD. As shown in Fig. 8, the cross section of the internal baffle narrows from the bottom to the top. If the bottom of the VD is equipped with a series of internal baffles, the bed materials inside the VD will fall down through the space between each two adjacent internal baffles slowly. The detailed design information of one internal baffles is presented in Fig. 8. The length of each internal baffle is 40 mm. The length of the bottom space of the VD is 624 mm. Hence, the internal baffles occupy 64.1% of the cross section at the bottom of the VD.

2.3. Operational conditions

This study used glass beads as bed material, with a density of 2600 kg/m^3 and a particle size range from 250 μm to 425 μm. These solids belong to Group B in the Geldart classification. The average particle diameter is 316 μm. In each experiment, 100 kg solids were filled into the riser, yielding a fixed bed height around 0.5 m.

The experiments were conducted with the VD equipped with/without the internal baffles and different air distributors (AD198 and AD1660) at different fluidization velocities and simulated volatiles flowrates. The air distributors used in this work are perforated plates with different open areas, one with 198 holes (AD198) and the other one with 1660 holes (AD1660). The holes have a diameter of 2 mm. Different flowrates of the simulated volatiles represent different fuel feed rate in real application to some extent. Different fluidization velocities and air distributors are adopted to create different fluidization regimes in the riser. Further, the gas flow in the fuel reactor changes over the height. It is also motivated to investigate the performance of the VD under different fluidization velocities [9,11]. The cases without VD are reference cases to assess the improvement of the horizontal distribution by the VD. The injection port is the same one in all cases. The operational conditions are presented in Table 1.

2.4. Data analysis

2.4.1. Pressure analysis

The vertical profile of the solids concentration is obtained from the pressure measurements along the height of the riser. The average solids concentration between two heights is calculated by the pressure drop over the height interval [34]. First, the voidage is solved from the general expression for the pressure drop.

$$\Delta p = \left(\rho_s(1-\varepsilon_g) + \rho_g\varepsilon_g\right)g(h_1 - h_2) \tag{1}$$

Then, the average solids concentration in this height interval can be calculated as:

$$c_s = \rho_s(1-\varepsilon_g) \tag{2}$$

The average values and standard deviation of the pressures inside and outside the VD are calculated based on the pressure data recorded for 2730 s with the frequency 50 Hz.

$$\overline{P} = \frac{\sum_{n=1}^{N} x(n)}{N} \tag{3}$$

$$\sigma = \sqrt{\frac{\sum_{n=1}^{N}(x(n) - \overline{P})^2}{N}} \tag{4}$$

where $\overline{P}$ is the average value, N is the total number of the data points and $n = 1, 2, 3, \ldots, N$.

The dense bed height inside the VD, h_b, can be estimated from the pressure drop over the distribution holes, $p_{in} - p_{out}$, and the measured pressure gradient outside the VD. Assuming similar pressure gradient inside and outside the VD, the distance between the dense bed surface and the level of the distribution holes, i.e. Δh, can be calculated as:

$$\Delta h = \frac{p_{in} - p_{out}}{|dp/dh|} \tag{5}$$

The geometry in Fig. 9 gives:

$$h_b = h_{hole} - \Delta h - h_{bottom} \tag{6}$$

The values of h_{bottom} and h_{hole} are shown in Fig. 5 (b).

2.4.2. CO_2 concentration analysis

In the ideal case, the injected simulated volatiles are distributed

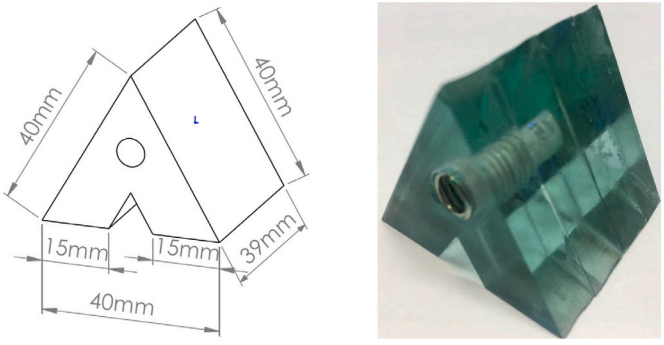

Fig. 8. Internal baffle (shown at the bottom of VD in Fig. 6).

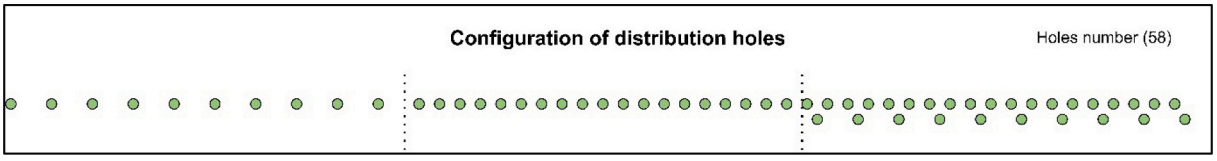

Fig. 7. The configuration of distribution holes of the volatiles distributor (referred to Mode 1B in the reference [10]).

Table 1
Operational conditions with different air distributors.

Air distributor			AD198						AD1660					
Fluidization velocity	u_0	m/s	0.6						0.6			3.7		
Internal baffles			Reference	Without	With	Reference	Without	With	Reference	Without	With	Reference	Without	With
Primary air flow	V_{pa}	m_n^3/h	166	165	163	166	166	166	167	166	166	967	971	973
CO_2 flow	V_{CO_2}	L_n/min	13.0	13.0	13.0	30.0	30.0	23.0	13.0	13.0	13.0	20.0	22.4	20.0
Air for simulated volatiles	V_{sa}	m_n^3/h	76	69	71	126	120	121	71	70	73	113	109	109
Simulated volatiles	V_{sv}	m_n^3/h	77	70	71	128	122	123	72	71	73	114	111	111
Volatiles percentage	$\frac{V_{sv}}{V_{pa}+V_{sv}}$		32%	30%	30%	44%	42%	42%	30%	30%	31%	11%	10%	10%

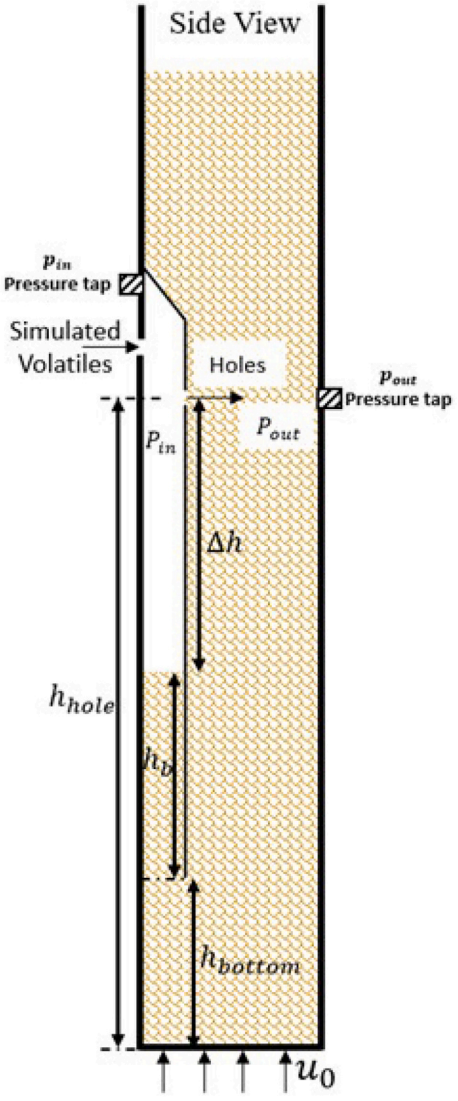

Fig. 9. Sketch of the side view of the riser bottom (refer to section c in Fig. 5).

evenly over the whole cross section of the main riser. Therefore, the expected tracer gas CO_2 concentration all over the cross section can be calculated as:

$$c_{cal} = \frac{MF_{CO_2}}{MF_{CO_2} + MF_{SA} + MF_{PA}} \tag{7}$$

In order to compare the tracer gas (CO_2) distribution of simulated volatiles in the horizontal cross section under different operating conditions, the CO_2 ratio concept is adopted in this work since there is always a slight difference in CO_2 concentration in the injected simulated volatiles under different conditions. The CO_2 ratio is defined as the ratio between the measured CO_2 concentration (c_m [ppm]) at each measurement position and the ideal average CO_2 concentration (c_{cal} [ppm]) in the cross-section of the riser based on Eq. (7).

$$R = \frac{c_m}{c_{cal}} \tag{8}$$

In order to evaluate statistically the overall performance of the VD with and without the internal baffles under different experimental conditions, a further analysis is conducted of the CO_2 ratios at the six higher-level horizontal measurement positions, which includes the average CO_2 ratio ($\bar{c}$), the standard deviation of the CO_2 ratios (*SD*), relative standard deviation of the CO_2 ratios (*RSD*), and the ratio

between the highest CO_2 ratio and the lowest CO_2 ratio (H/L). The calculations on the above parameters are shown as:

$$\overline{R}(R_1, R_2, \ldots R_n) = \frac{\sum_{i=1}^{n} R_i}{n} \tag{9}$$

$$SD = \sqrt{\frac{\sum_{i=1}^{n} (R_i - \overline{R})^2}{n}} \tag{10}$$

$$RSD = \frac{SD}{\overline{R}} \times 100\% \tag{11}$$

$$H \Big/ L = \frac{R_{highest}}{R_{lowest}} \tag{12}$$

2.4.3. The dilution of volatiles inside the VD

The injected simulated volatiles could be diluted by the bottom air from the main fluidization. This dilution affects the horizontal distribution of the simulated volatiles. Therefore, the flow of fluidization air from the bottom entering the VD is estimated in this work.

The method is based on the calculation of the gas velocity through the orifice [35]. Once the pressure drop over the distribution holes, $p_{in} - p_{out}$, and the orifice discharge coefficient, C_d, are known, the gas velocity through the distribution holes can be estimated.

$$v_{orifice} = C_d \sqrt{\frac{2(p_{in} - p_{out})}{\rho_g}} \tag{13}$$

- Here, the gas density, $\boldsymbol{\rho_g}$, is 1.19 kg/m^3, and the value of $\boldsymbol{C_d}$ depends on the grid plate thickness, t, and the hole pitch, L_h. According to the relationship between $\boldsymbol{C_d(L_h/d_h)^{0.1}}$ and thickness-to-diameter ratio in the design chart for the grid hole's discharge coefficient design chart [36], where $\boldsymbol{d_h}$ is the diameter of the holes, the value of $\boldsymbol{C_d}$ can be set to 0.92, since L_h, d_h and t are 10 mm, 5 mm, and 8 mm respectively.

Then, the total gas flow through the distribution holes is obtained knowing the open area $A_{orifice}$, which is 1.138×10^{-3} m^2.

$$V_{orifice} = v_{orifice} \times A_{orifice} \tag{14}$$

The total gas flow through the distribution holes of the VD ($V_{orifice}$) includes the bottom air flow (V_{ba}) and the flow of injected simulated volatiles (V_{sv}). Hence, the bottom air flow is estimated as:

$$V_{ba} = V_{orifice} - V_{sv} \tag{15}$$

The simulated volatiles injected into the VD can be diluted by the bottom air from the main riser. The dilution may have an impact on the horizontal distribution and the performance of the VD. The dilution can be estimated based on two methods. The first method is to calculate the ratio between the bottom air flow and the injected simulated volatiles flow. The second method is to calculate the ratio between the measured CO_2 concentration inside the VD and the CO_2 concentration of the injected simulated volatiles. Based on the above two methods, the dilution factors can be calculated as:

$$D_1 = \frac{V_{ba}}{V_{sv}} \tag{16}$$

$$D_2 = \frac{c_{vd}}{c_{sv}} = \frac{c_{vd}}{V_{CO_2}/V_{sv}} \tag{17}$$

Here, c_{vd} is the measured CO_2 concentration inside the VD at the top right corner.

3. Results and discussion

3.1. Observation of the dense bed inside the VD

Table 2 shows photos of the fluidization inside the VD captured from the front window under different operational conditions. In the case with AD1660 and without internal baffles, there are big bubbles formed at the bottom when the fluidization velocity is low, which push particles upwards to the top of the VD. When the air distributor is changed to AD198, there are multiple and smaller bubbles formed at the bottom and the dense bed oscillates less violently than the cases with AD1660. The dense bed surface becomes more stable by the installation of the internal baffles with the high pressure drop AD198. For the cases with internal baffles at lower fluidization velocities in Table 2, the internal baffles break the large bubbles, and the movement of particles is reduced by the internal baffles, which help creating a more stable dense bed inside the VD.

As the fluidization velocity increases to 3.7 m/s, the bed inside the VD is more diluted and the bed height remains lower and more unevenly distributed in the lateral direction compared to the lower fluidization velocity cases. Note that the inner wall of the VD is also made in perplex, so in the photos with low bed levels, the fluidization behavior of the bed behind, i.e. outside of the VD, can be also seen. There is very little dense bed observed in the case with internal baffles at high fluidization velocity.

Videos from the ten cases shown in Table 2 are available on the internet [37], and these provide better comparisons of the gas/solid movements inside the VD.

3.2. Effects of the internal baffles on the solids concentration profile

As indicated in the previous work different air distributors, i.e. AD198 and AD1660, could result in different fluidization regimes at small fluidization velocities [10]. In the cases investigated in this work, single bubble regime and multiple bubble regime [38] are achieved by AD1660 and AD198 respectively. The exploding bubble regime [38] is achieved by increasing the fluidization velocity to 3.7 m/s with AD1660. The single bubble and multiple bubble regimes achieve similar solids concentration as shown in Fig. 10. In contrast, the exploding bubble regimes with the higher fluidization velocity has much lower solids concentration at the bottom of the riser, i.e. below the height of 0.92 m, as shown by the red lines in Fig. 10.

However, there is no obvious difference in the solids concentration when the simulated volatiles flow is increased. Similarly, there is no significant effect on the solids concentration by installing the internal baffles on the VD.

3.3. Effects of the internal baffles on the pressures inside and outside the VD

The effects of internal baffles on the pressures inside and outside the VD are analyzed according to the comparisons in Table 3. In the multiple bubble regime, i.e. AD198, the pressure inside the VD decreases slightly and the pressure outside the VD increases after the installation of the internal baffles, which results in a decrease of the pressure drop, i.e. $p_{in} - p_{out}$. Similar decrease in the pressure drop is found in the single bubble regime. However, in the single bubble regime, the pressure inside the VD decreases significantly and the pressure outside the VD decreases slightly. Compared to the multiple bubble regime, the dense bed inside the VD fluctuates more violently due to the larger bubbles formed in the single bubble regime in the absence of baffles. Less bottom air takes the path through the VD and its distribution holes and more bed material stays inside the VD with the internal baffles compared to the cases without internal baffles. This decreases the pressure drop between the inside and outside of the VD and gives a higher bed level inside the VD in both multiple and single bubble regimes.

Table 2
Photographs of the dense bed inside the VD under different operational conditions.(Views refer to section B in Fig. 5).

Air distributor	Internal baffle	u_0 = 0.6 m/s, V_{sv}~30%	u_0 = 0.6 m/s, V_{sv}~42%	u_0 = 3.7 m/s, V_{sv}~10%
AD1660	Without	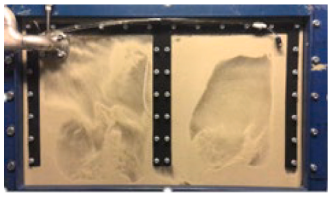 (a)	 (b)	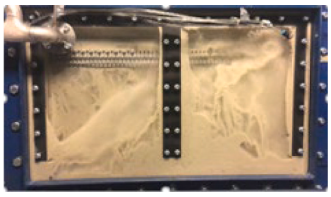 (c)
	With	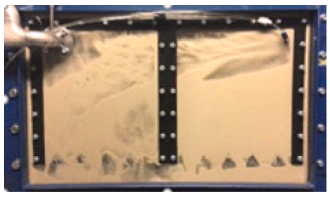 (d)	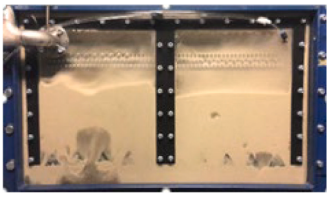 (e)	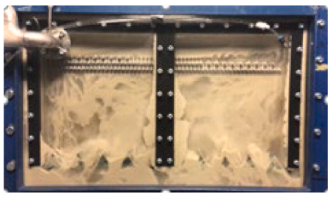 (f)
AD198	Without	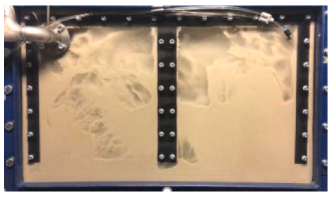 (g)	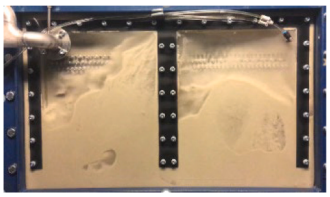 (h)	
	With	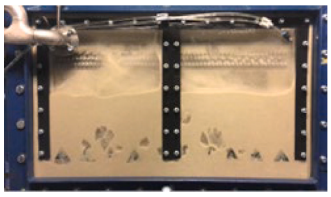 (i)	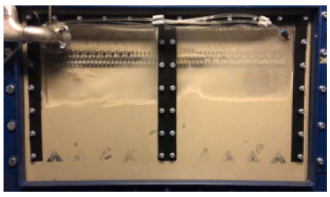 (j)	

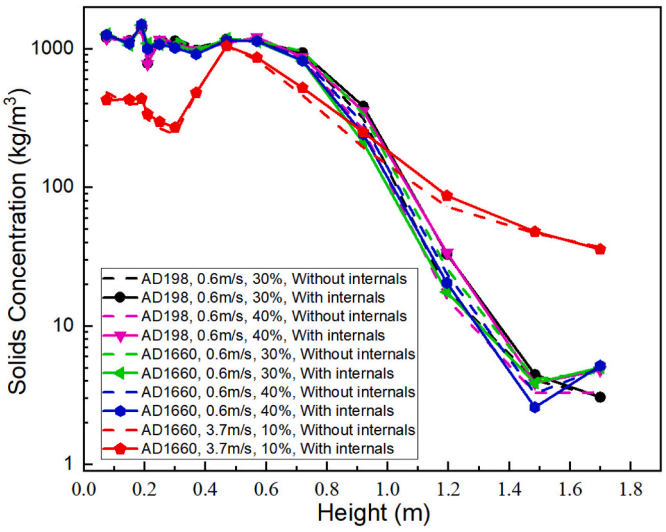

Fig. 10. Solids concentration profiles at riser bottom under different operational conditions. (With/Without refer to internal baffles.)

In the exploding bubble regime, pressures both inside and outside of the VD increase slightly by addition of the internal baffles as shown in Table 3, which causes similar pressure drops over the distribution holes in both cases with and without the internal baffles.

The correlation between the pressures inside and outside of the VD was analyzed based on the CORREL function in Excel. The correlation coefficient is used to determine how well the pressure inside and outside of the VD are correlated. The correlation coefficient closer to 0 means that these two parameters are less correlated. When the correlation coefficient is approaching to 1, these parameters are correlated tightly. As shown in Table 3, the correlation coefficient in multiple bubble regime is much lower than the other two regimes, which causes a higher standard deviation of the pressure drop over the distribution holes of the VD.

3.4. *Effects of the internal baffles on the horizontal distribution of the volatiles*

3.4.1. *Tracer gas concentration distribution*

Fig. 11 shows the concentration of the tracer gas, i.e. CO_2, at different measurement positions (LSV1–6/HSV1–6) during the 120 s recording time under the multiple bubble regime. Comparison with the reference case, i.e. VD without internal baffles, shows that the use of baffles yields a more uniform horizontal distribution of volatiles, except at HSV1, the position closest to the simulated injection port.

3.4.2. *CO_2 ratio distribution*

A comparison between the cases with and without internal baffles in the multiple bubble regime, Fig. 12 (a), clearly shows that the horizontal distribution of CO_2 is improved by the internal baffles. The CO_2 ratios on the left side, near the simulated volatiles injection port, are lowered and the ones at the right side, the opposite side to the injection port, are increased to the average level as a consequence of the internal baffles. There is essentially no CO_2 detected at the lower level, which means that

Table 3
Influence of internal baffles on the pressures inside and outside the VD.

Air distributor			AD198				AD1660					
Fluidization velocity	u_0	m/s	0.6				0.6				3.7	
Volatiles percentage	$\frac{V_{sv}}{V_{pa}+V_{sv}}$		30%		42%		30%–31%		42%		10%	
Fluidization regime			Multiple bubble				Single bubble				Exploding bubble	
Internal baffles			No baffles	Baffles	No baffles	Baffles	No baffles	Baffles	No baffles	Baffles	No baffles	Baffles
Pressure inside VD	p_{in}	kPa	6.47	6.33	6.74	6.67	6.82	5.74	7.04	6.26	7.06	7.32
Standard deviation of p_{in}	$std_{p_{in}}$	kPa	1.50	1.65	1.63	1.81	1.36	1.71	1.39	1.04	0.62	0.72
Pressure outside VD	p_{out}	kPa	5.25	5.50	5.01	5.37	5.38	4.81	5.09	4.89	6.07	6.31
Standard deviation of p_{out}	$std_{p_{out}}$	kPa	0.49	0.44	0.42	0.35	1.15	1.34	1.16	1.32	0.69	0.80
Correlation coefficient between $p_{in}$and p_{out}	–	–	0.42	0.38	0.37	0.33	0.69	0.79	0.65	0.77	0.82	0.84
Pressure drop over the VD	$p_{in}-p_{out}$	kPa	1.21	0.83	1.73	1.29	1.43	0.93	1.95	1.37	0.99	1.01
Standard deviation of $p_{in}-p_{out}$	$std_{p_{in}-p_{out}}$	kPa	1.38	1.55	1.53	1.74	1.01	1.03	1.09	1.04	0.36	0.37
Pressure gradient	dp/dh	kPa/m	10.66	10.56	10.39	10.38	10.73	10.30	10.32	10.13	4.24	4.16
Dense bed height inside VD	h_b	m	0.15	0.18	0.09	0.14	0.13	0.17	0.07	0.12	0.03	0.02

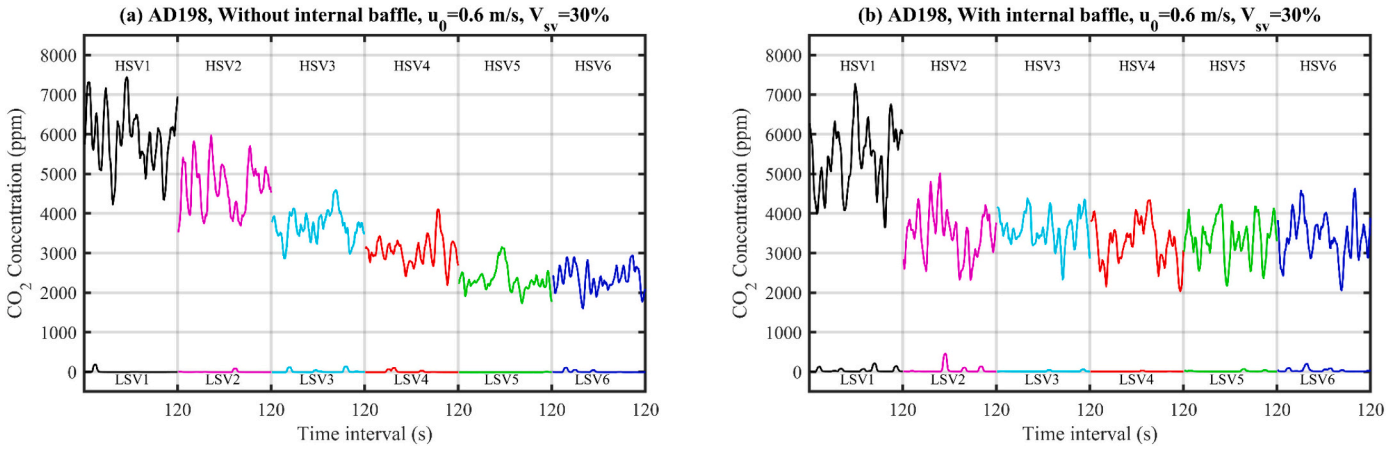

Fig. 11. An example of CO_2 concentration signals at different measurement positions with and without internal baffles under the multiple bubble regime.

there is neither any gas back-mixing nor any bottom leakage from underneath of the VD.

Similarly, the horizontal distribution of simulated volatiles is more even with the VD equipped with internal baffles in the single bubble regime compared to the one without internal baffles as presented in Fig. 12 (b). In particular, the CO_2 ratios at the right side, i.e. far away from the injection side, are improved significantly by the internal baffles and the VD.

However, the CO_2 ratios measured at the lower level with the VD equipped with internal baffles are higher than the ratios in the cases without internal baffles and the reference cases without VD denoted as blank in Fig. 12 (b). By comparison of the red and yellow dashed lines in Fig. 12 (b), the CO_2 ratios at LSV1 and LSV2 for different fractions of the simulated volatiles are similar, which means that the increase of the flowrate of simulated volatiles does not give any effect on the CO_2 ratios at the lower level. Hence, the larger CO_2 ratios at LSV1 and LSV2 with the VD equipped with internal baffles, i.e. the red and yellow dashed lines in Fig. 12 (b), compared to the ratios without internal baffles, are estimated to be caused by enhanced gas back-mixing due to the installation of internal baffles instead of bottom leakage.

As shown in Table 2, there are large bubbles formed in the core region inside the VD in the reference case with AD1660 and 0.6 m/s fluidization velocity. Therefore, there should be similar large bubbles formed behind the volatiles distributor plate in the main riser. In the core region, the large bubble tends to rise carrying solids in the wakes and the bubble fraction is large, resulting in less downward solids flux. In the wall region, descending solids replace the upward-moving solids in the core region. The bubble fraction is low and most solids descend. Hence, a core wall-layer structure is formed at the bed bottom [39]. There are several parameters, i.e. molecular diffusion, turbulent gas diffusion and solids mixing, affecting the gas mixing in the fluidized bed. The downflow of solids in the wall region is the main reason for the gas back-mixing [39,40]. As shown in Table 5, there is more fluidization air flowing upwards in the main riser instead of flowing into the VD after the installation of internal baffles. More ascending fluidization air could cause larger bubbles to carry more solids upwards in the core region and larger downflow of solids in the wall region to replace the asceding solids in the core region. The larger downflow of solids enhances the gas back-mixing in the wall region and leads to the higher CO_2 ratios at LSV1 and LSV2 in the cases with internal baffles. Strong support for this interpreation is that higher CO_2 ratios are seen both at the right and left side in Fig. 12 (b), whereas it is approaching zero in the middle.

In the previous work [9], it was observed that the effect of the VD on the horizontal distribution is improved by increasing the simulated volatiles flow. After the installation of the internal baffles on the VD, the performace of the VD is similar in both single and multiple bubble regimes regardless of the simulated volatiles flow, even though the pressure drop over the VD distribution holes is increased by increasing the simulated volatiles flow as indicated in Fig. 12 (a) and (b).

In the exploding bubble regime, the CO_2 ratio at the left side is

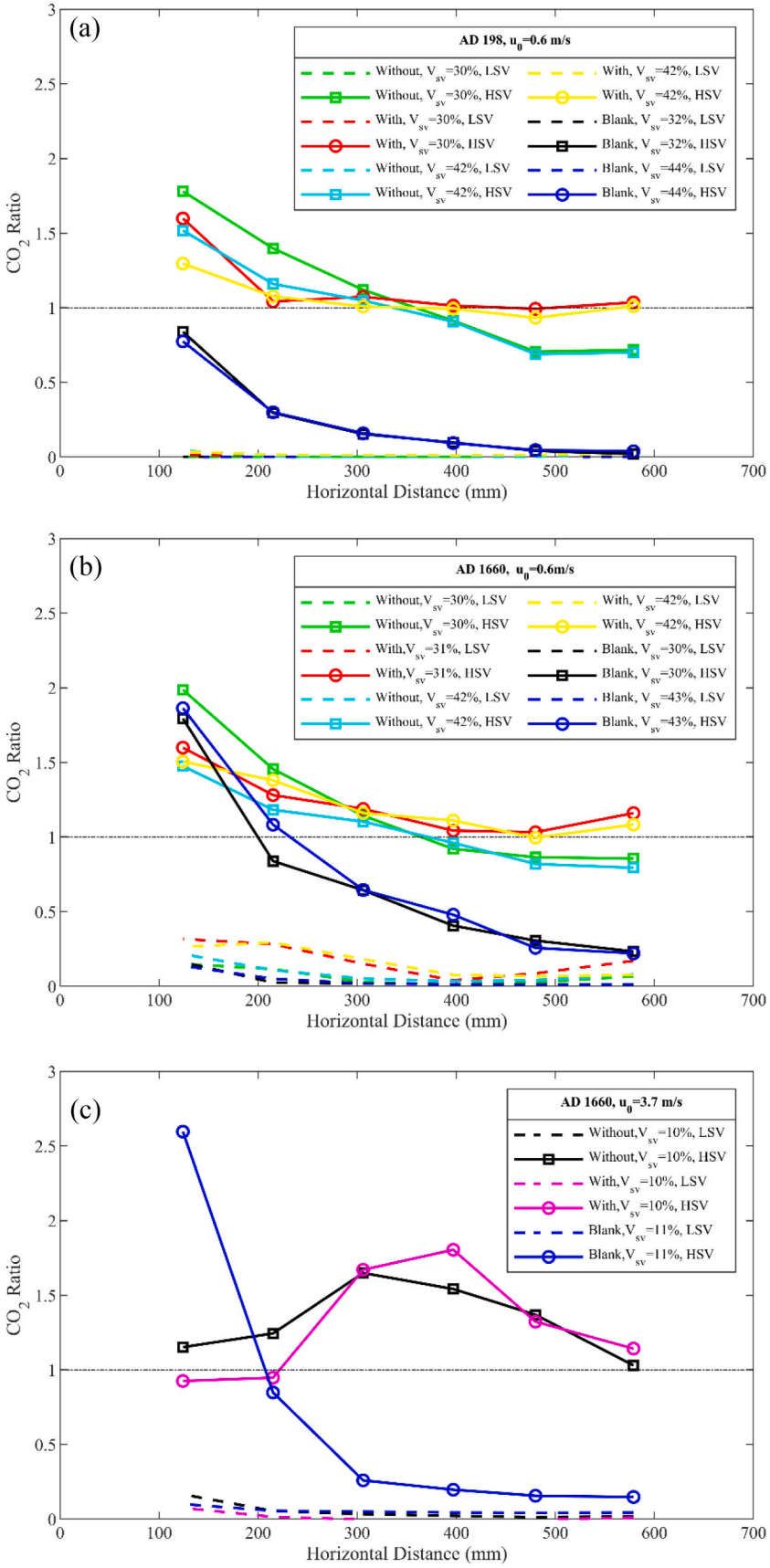

Fig. 12. The distribution of tracer gas in the horizontal direction from the left side of the riser under different operating conditions. ('Blank', 'with' and 'without' refer to 'reference case without VD', 'VD with internal baffles' and 'VD without internal baffles' respectively.)

lowered slightly and the one at the right side is higher with the VD equipped with internal baffles compared to the case without internals as shown in Fig. 12 (c). In total, the distribution is somewhat worsened with baffles. On the other hand, the data clearly show a displacement of gas from the inlet at the left to the right, indicating that the VD is too efficient in moving the gas away from the inlet. This can of course be solved by moving the holes from the right to left, c.f. Fig. 7. The performance of the VD with internal baffles is similar to the one without internals. However, the VDs did significantly improve the uniformity of the horizontal gas distribution compared to the reference case without VD.

3.4.3. Statistical analysis on performance of internal baffles

Table 4 shows statistically the overall performance of the VD with and without internal baffles under different operational conditions. In the multiple and single bubble regimes, the standard deviation, and relative standard deviation of the CO_2 ratios, together with the highest/lowest concentration, are much lower in the cases with internal baffles. This result is consistent with the observations that can be made from Fig. 12.

In the exploding bubble regime, the standard deviation, the relative standard deviation and the highest/lowest concentration of CO_2 ratios are higher in the case with internal baffles compared to the case without baffles. This can be explained by lower the CO_2 ratios at HSV1 and HSV2 and higher ones at HSV4 and HSV5 in the case with internal baffles compared to the case without baffles, which means that the installation of the internal baffles help the VD push more simulated volatiles to be distributed from the side further away from the simulated volatiles injection port. Thus, the internal baffles do not improve the distribution of the simulated volatiles distribution in the exploding bubble regime, but it amplifies the movement of volatiles away from the injection port which is the purpose of the uneven hole distribution. This means that the internal baffles facilitate the control over the distribution, which is an important point considering the application in longer VD arms.

It is shown in Table 4 that the standard deviation, relative standard deviation, and the highest/lowest concentration are much lower when the volatiles percentage increases in the single and multiple bubble regime for the reference cases without internal baffles. However, these values remain similar in the cases with internal baffles, especially in the single bubble regime, which means that once the internal baffles are installed, the flowrate of simulated volatiles would not have a big impact on the horizontal distribution by the VD.

3.5. Effects of the internal baffles on the volatiles dilution inside the VD

Table 5 presents the calculation results of the simulated volatiles dilution inside the VD according to the orifice discharge coefficient equation, cf. Eqs. (13), (14) and (15). The dilution factors, i.e. V_{ba}/V_{sv} and c_{vd}/c_{sv} are analyzed based on the Eq. (16) and Eq. (17).

The volatiles injected into the VD are diluted by the bottom air flowing into the VD. As Table 5 shows, when the internal baffles are installed in the VD, there is less bottom air flowing into the VD and the dilution of the injected simulated volatiles is smaller, especially in the single and multiple bubble regime. However, there is no big difference in the volatiles dilution inside the VD, i.e. the bottom air flow or fluidization velocity inside the VD before and after the installation of the internal baffles in the exploding bubbling regime. But more simulated volatiles can be moved away from injection port to the right side with the help of internal baffles.

3.6. Implications for large-scale application of the VD

The investigation of the VD with different configurations has been made in a cold-flow fluidized-bed model under varying fluidization regimes. The performance of the VD in the cold-flow model gives some hints for the performance of the VD in a real-world application with the same fluidization regime. But, what would be the expected operational conditions in a future fuel reactor using solid fuels? There are some differences between the operational conditions in current investigations in the cold-flow model and the ones in the large-scale fuel reactors.

Firstly, the bottom fluidization gas flow would be low in a real-world fuel reactor. The bottom gas, either steam or a combination of steam and recycled CO_2, comes with a significant cost, and its major purpose is to keep the bed fluidized. Thus, the optimal bottom gas flow is likely the minimum flow needed to safely achieve adequate fluidizing conditions. Apart from the bottom fluidization gas flow, there are two major gas flows in the fuel reactor originating from the char and the volatiles. The char will mainly be part of the dense phase. Thus, the syngas produced by gasification will also appear in the dense phase. This will make the dense phase "self-fluidizing", which is likely helpful for improving the gas-solid contacting. It also means that the gas flow in the dense phase outside the VD will increase with bed height. Such a "self-fluidizing" is obviously difficult to be accomplished in a cold-flow model. Therefore, it is relevant to consider different fluidization velocities in the evaluation, i.e. from the low velocities, typical of the fluidization flow, to the higher flows which are more relevant higher up in the bed.

A second difference is that the flow of volatiles in a fuel reactor which uses a highly volatile biomass fuel, would be significantly higher than that used in these tests in the cold-flow model. This was caused by practical limitations to the flow that could be added. In large-scale units, the flow of volatiles depends on the fuel injection position, the properties of the fuel and the extent of devolatilization. In a conceptual design of 1000 MW_{th} boiler for chemical-looping combustion of solid fuel, the solid fuel is injected between the downcomer and the fuel reactor [11], which should give enough time for the devolatilization process. So with a constant fuel feed rate, the volatiles flow should be stable. Further, different designs of the VD, i.e. the distance between the distribution holes and the lower edge of the VD, the arrangement and open area of the distribution holes, can be used to optimize the VD and provide the operational flexibility. The use of a higher flow in this work would obviously have implications for the dimensioning of the arms and the open area of the holes.

Another difference is the relative size of the VD compared to the fluidized bed in the cold-flow model and in real-world application. The solids distribution, i.e. solids concentration, in the bottom region is affected by the installation of the VD, especially when the overall

Table 4
General performance of the VD with and without internal baffles under different operation conditions.

Air distributor	Fluidization velocity	Fluidization regime	Volatiles percentage	Average CO_2 ratio		Standard deviation		Relative standard deviation		Highest/Lowest concentration	
	m/s			No baffles	Baffles	No baffles	Baffles	No baffles	Baffles	No baffles	Baffles
AD198	0.6	Multiple bubble	30%	1.11	1.13	0.38	0.21	0.35	0.19	2.52	1.61
			42%	1.00	1.05	0.29	0.12	0.29	0.11	2.20	1.39
AD1660		Single bubble	30–31%	1.20	1.22	0.41	0.19	0.34	0.16	2.30	1.55
			42%	1.06	1.21	0.23	0.18	0.22	0.15	1.80	1.51
	3.7	Exploding bubble	10%	1.33	1.30	0.21	0.34	0.16	0.26	1.60	1.95

Table 5
Volatiles dilution inside the VD estimated based on orifice discharge coefficient.

Air distributor	Fluidization velocity	Fluidization regime	Volatiles percentage	Internal Baffle	Pressure drop over the VD	$v_{orifice}$	V_{ba}	u_{VD}	c_{vd}	Dilution Factors	
					kPa	m/s	m_n^3/h	m/s	ppm	V_{ba}/V_{sv}	c_{vd}/c_{sv}
AD198	0.6 m/s	Multiple bubble	30%	No baffles	1.21	41.52	100.11	1.17	4934	1.43	0.44
				Baffles	0.83	34.44	69.72	0.82	8267	0.98	0.76
			40%	No baffles	1.73	49.61	81.11	0.95	10,365	0.66	0.70
				Baffles	1.29	42.91	53.27	0.62	10,327	0.43	0.92
AD1660	0.6 m/s	Single bubble	30%	No baffles	1.43	45.20	114.51	1.34	5829	1.62	0.53
				Baffles	0.93	36.42	75.88	0.89	8421	1.03	0.79
			40%	No baffles	1.95	52.73	98.31	1.15	7558	0.84	0.67
				Baffles	1.37	44.13	57.31	0.67	9213	0.46	0.90
	3.7 m/s	Exploding bubble	10%	No baffles	0.99	37.49	42.92	0.50	9123	0.39	0.75
				Baffles	1.01	37.92	44.84	0.53	8578	0.41	0.79

fluidization velocity is high [9]. This is because the VD occupies one third of the riser cross-section. However, the influence of the installation of the VD on the solids concentration is expected to be less in real-world application since the arms of the volatiles distributor would cover a smaller fraction of the cross-section of fluidized beds.

Despite these differences, it can be concluded that the concept of the VD has been proven and can be expected to be useful in real-world applications. Moreover, the different configurations and conditions examined in this work should be helpful in the design of large-scale applications.

4. Conclusion

In this work, the influence of internal baffles on the performance of a volatiles distributor is investigated, in particular in the horizontal distribution of volatiles and the volatiles slip from the bottom of the volatiles distributor.

It is obvious that the installation of the internal baffles inside the VD improves the horizontal distribution of simulated volatiles achieved by the VD in the single and multiple bubble regimes. Much higher concentration of simulated volatiles is found at the far end of the distributor as viewed from the volatiles injection side. Also, in the exploding bubble regime, the volatiles are moved away from the inlet. In this case, it leads to a less even distribution, which should be easy to address by having more distribution holes to the left. Thus, the results consistently show that the internal baffles promote the transfer of volatiles away from the volatiles inlet. This means that the baffles facilitate the redistribution of volatiles which is the purpose of the volatiles distributor.

Higher simulated volatiles flowrate can improve the horizontal gas distribution by the VD without internal baffles. Once the internal baffles are installed inside the VD, the benefit for uniformity of the horizontal gas distribution by increasing the simulated volatiles flowrate is not obvious anymore.

The installation of internal baffles reduces the bottom air flowing into the VD. Furthermore, the baffles seem to enhance the gas backmixing outside the VD. which causes a higher simulated volatiles concentration at the lower level of the VD. The higher concentration is likely not explained by the bottom leakage, since there is no change in the concentration when the simulated volatiles flowrate is increased.

In general, the volatiles distributor could improve the horizontal gas distribution significantly. However, perhaps the performance of the volatiles distributor is poor due to the volatiles slip from the bottom of the volatiles distributor near the volatiles injection side, especially in the single bubble regime, which has more violent bed surface fluctuations inside the volatiles distributor. This problem of volatiles slip from the bottom might be more obvious in the large-scale fluidized bed, i.e. for a larger cross section and a longer volatiles distributor. Hence, the installation of the internal baffles at the bottom of the VD could be a solution to volatiles slip from the bottom of the VD, in particular for the single bubble regime in the larger scale fluidized bed. In the meantime, the internal baffles can also make positive effects on the uniformity of the horizontal gas distribution by the volatiles distributor.

Nomenclatures

Abbreviations

AD198	The air distributor with 198 holes
AD1660	The air distributor with 1660 holes
BECCS	Bioenergy carbon capture and storage
Bio-CLC	Chemical looping combustion of biomass
CLC	Chemical looping combustion
CLOU	Chemical looping with oxygen uncoupling
HSV	High-level sampled volatiles
LSV	Low-level sampled volatiles
OC	Oxygen carriers
VD	Volatiles distributor

Notations

$A_{orifice}$	Open area of the orifices/distribution holes of the VD [m^2]
c_{cal}	Expected average CO_2 concentration in the cross-section of the riser [ppm]
c_m	Measured CO_2 concentration [ppm]
c_{vd}	CO_2 concentration measured inside VD [ppm]
c_{sv}	CO_2 concentration in the simulated volatiles [ppm]
C_d	Orifice discharge coefficient [−]
c_s	Average solids concentration in a height interval [kg/m^3]
d_h	Diameter of the distribution hole [mm]
dp/dh	Pressure drop gradient [kPa/m]
D_1, D_2	Dilution factors calculated based on two methods [−]
g	Acceleration of gravity [m/s^2]
h_1, h_2	Different heights of the pressure measurement positions [m]
h_b	Dense bed height inside volatiles distributor [m]
h_{bottom}	Height of the bottom of the volatiles distributor [m]
h_{hole}	Height of the distribution holes [m]
Δh	Height difference between the height of the distribution holes and the dense bed surface inside the VD [m]
H/L	Ratio between the highest CO_2 ratio and the lowest CO_2 ratio [−]
L_h	Pitch of the distribution hole [mm]
MF_{CO_2}	CO_2 flow [m_n^3/h]
MF_{SA}	Air flow used for simulating volatiles [m_n^3/h]
MF_{PA}	Primary air flow for the main fluidization [m_n^3/h]
N	Total number of the pressure data points [−]
Δp	Pressure drop over a height interval [kPa]
P_{in}	Pressure inside the VD measured at the top right corner [kPa]
P_{out}	Pressure outside the VD measured at the back side of the riser

	at the distribution holes level [kPa]
$\overline{P}$	Average pressure [kPa]
R	CO_2 ratio [−]
$\overline{R}$	Average CO_2 ratio [−]
R_i	CO_2 ratios at different horizontal positions [−]
$R_{highest}$	Highest CO_2 ratio over the six measurement positions [−]
R_{lowest}	Lowest CO_2 ratio over the six measurement positions [−]
RSD	Relative standard deviation of the CO_2 ratios [−]
$std_{p_{in}}$	Standard deviation of p_{in} [kPa]
$std_{p_{out}}$	Standard deviation of p_{out} [kPa]
$std_{p_{in}-p_{out}}$	Standard deviation of $p_{in} - p_{out}$ [kPa]
SD	Standard deviation of the CO_2 ratios [−]
t	Thickness of the grid plate [mm]
u_0	Fluidization velocity [m/s]
u_{VD}	Fluidization velocity inside the VD based on two calculation methods [m/s]
$v_{orifice}$	Gas velocity through the orifice [m/s]
V_{ba}	Bottom air flow from the main riser to the VD [m_n^3/h]
V_{CO_2}	CO_2 flowrate [m_n^3/h]
V_{pa}	Primary air flowrate [m_n^3/h]
V_{sa}	Secondary air flowrate for simulating volatiles [m_n^3/h]
V_{sv}	Simulated volatiles flowrate [m_n^3/h]
$V_{orifice}$	Orifice gas flow [m_n^3/h]
$x_i(n)$	Time serials of pressure signals [kPa]
ρ_g	Density of fluidization gas [kg/m^3]
ρ_s	Density of solid bed materials [kg/m^3]
σ	Standard deviation of pressures [kPa]
ε_g	Gas voidage [−]

CRediT authorship contribution statement

Xiaoyun Li: Conceptualization, Methodology, Validation, Formal analysis, Investigation, Writing – original draft, Writing – review & editing. **Anders Lyngfelt:** Conceptualization, Writing – review & editing, Supervision, Funding acquisition. **Carl Linderholm:** Validation, Writing – review & editing, Supervision. **Bo Leckner:** Writing – review & editing. **Tobias Mattisson:** Writing – review & editing, Supervision.

Declaration of Competing Interest

The authors declare that they have no known competing financial interests or personal relationships that could have appeared to influence the work reported in this paper.

Acknowledgements

This work was funded by the Swedish Energy Agency, project number 46626-1.

References

[1] V. Masson-Delmotte, et al., IPCC, 2021: summary for policymakers, in: Climate Change 2021: The Physical Science Basis. Contribution of Working Group I to the Sixth Assessment Report of the Intergovernmental Panel on Climate Change, 2021 (In Press).
[2] M. Rydén, A. Lyngfelt, Ø. Langørgen, Y. Larring, A. Brink, S. Teir, H. Havåg, P. Karmhagen, Negative CO2 emissions with chemical-looping combustion of biomass – a Nordic Energy Research flagship project, Energy Procedia 114 (2017) 6074–6082, https://doi.org/10.1016/j.egypro.2017.03.1744.
[3] R. Solimene, R. Chirone, P. Salatino, Characterization of the devolatilization rate of solid fuels in fluidized beds by time-resolved pressure measurements, AICHE J. 58 (2) (2012) 632–645, https://doi.org/10.1002/aic.12607.
[4] H. Luo, Z. Lu, P.A. Jensen, P. Glarborg, W. Lin, K. Dam-Johansen, H. Wu, Experimental and modelling study on the influence of wood type, density, water content, and temperature on wood devolatilization, Fuel 260 (2020), 116410, https://doi.org/10.1016/j.fuel.2019.116410.
[5] N. Berguerand, A. Lyngfelt, Design and operation of a 10 kWth chemical-looping combustor for solid fuels – testing with south African coal, Fuel 87 (12) (2008) 2713–2726, https://doi.org/10.1016/j.fuel.2008.03.008.
[6] A. Abad, I. Adánez-Rubio, P. Gayán, F. García-Labiano, L.F. de Diego, J. Adánez, Demonstration of chemical-looping with oxygen uncoupling (CLOU) process in a 1.5kWth continuously operating unit using a Cu-based oxygen-carrier, Int. J. Greenh. Gas Contr. 6 (2012) 189–200, https://doi.org/10.1016/j.ijggc.2011.10.016.
[7] P. Markström, A. Lyngfelt, Designing and operating a cold-flow model of a 100kW chemical-looping combustor, Powder Technol. 222 (2012) 182–192, https://doi.org/10.1016/j.powtec.2012.02.041.
[8] J. Ma, H. Zhao, X. Tian, Y. Wei, S. Rajendran, Y. Zhang, S. Bhattacharya, C. Zheng, Chemical looping combustion of coal in a 5kWth interconnected fluidized bed reactor using hematite as oxygen carrier, Appl. Energy 157 (2015) 304–313, https://doi.org/10.1016/j.apenergy.2015.03.124.
[9] X. Li, A. Lyngfelt, T. Mattisson, An experimental study of a volatiles distributor for solid fuels chemical-looping combustion process, Fuel Process. Technol. 220 (2021), 106898, https://doi.org/10.1016/j.fuproc.2021.106898.
[10] X. Li, A. Lyngfelt, D. Pallarès, C. Linderholm, T. Mattisson, Investigation on the performance of volatile distributors with different configurations under different fluidization regimes, Energy Fuel (2022), https://doi.org/10.1021/acs.energyfuels.1c04159.
[11] A. Lyngfelt, B. Leckner, A 1000 MWth boiler for chemical-looping combustion of solid fuels – discussion of design and costs, Appl. Energy 157 (2015) 475–487, https://doi.org/10.1016/j.apenergy.2015.04.057.
[12] A. Lyngfelt, C. Linderholm, Chemical-looping combustion of solid fuels – status and recent progress, Energy Procedia 114 (2017) 371–386, https://doi.org/10.1016/j.egypro.2017.03.1179.
[13] T. Mendiara, L.F. de Diego, F. García-Labiano, P. Gayán, A. Abad, J. Adánez, On the use of a highly reactive iron ore in chemical looping combustion of different coals, Fuel 126 (2014) 239–249, https://doi.org/10.1016/j.fuel.2014.02.061.
[14] M. Schmitz, C. Linderholm, Chemical looping combustion of biomass in 10- and 100-kW pilots – analysis of conversion and lifetime using a sintered manganese ore, Fuel 231 (2018) 73–84, https://doi.org/10.1016/j.fuel.2018.05.071.
[15] T. Mendiara, L.F. de Diego, F. García-Labiano, P. Gayán, A. Abad, J. Adánez, Behaviour of a bauxite waste material as oxygen carrier in a 500Wth CLC unit with coal, Int. J. Greenh. Gas Contr. 17 (2013) 170–182, https://doi.org/10.1016/j.ijggc.2013.04.020.
[16] J. Haus, K. Lyu, E.-U. Hartge, S. Heinrich, J. Werther, Analysis of a two-stage fuel reactor system for the chemical-looping combustion of lignite and bituminous coal, Energy Technol. 4 (10) (2016) 1263–1273, https://doi.org/10.1002/ente.201600102.
[17] M. Schmitz, C.J. Linderholm, A. Lyngfelt, Chemical looping combustion of four different solid fuels using a manganese-silicon-titanium oxygen carrier, Int. J. Greenh. Gas Contr. 70 (2018) 88–96, https://doi.org/10.1016/j.ijggc.2018.01.014.
[18] R. Pérez-Vega, A. Abad, F. García-Labiano, P. Gayán, L.F. de Diego, M.T. Izquierdo, Adánez, Juan chemical looping combustion of gaseous and solid fuels with manganese-iron mixed oxide as oxygen carrier, Energy Convers. Manag. 159 (2018) 221–231, https://doi.org/10.1016/j.enconman.2018.01.007.
[19] T. Mattisson, A. Lyngfelt, H. Leion, Chemical-looping with oxygen uncoupling for combustion of solid fuels, Int. J. Greenh. Gas Contr. 3 (1) (2009) 11–19, https://doi.org/10.1016/j.ijggc.2008.06.002.
[20] H. Leion, T. Mattisson, A. Lyngfelt, Using chemical-looping with oxygen uncoupling (CLOU) for combustion of six different solid fuels, Energy Procedia 1 (1) (2009) 447–453, https://doi.org/10.1016/j.egypro.2009.01.060.
[21] I. Adánez-Rubio, I. Adánez-Rubio, A. Abad, P. Gayán, L.F. de Diego, J. Adánez, CLOU process performance with a cu-Mn oxygen carrier in the combustion of different types of coal with CO2 capture, Fuel 212 (2018) 605–612, https://doi.org/10.1016/j.fuel.2017.10.065.
[22] T. Mendiara, I. Adánez-Rubio, P. Gayán, A. Abad, L.F. de Diego, F. García-Labiano, J. Adánez, Process comparison for biomass combustion: in situ gasification-chemical looping combustion (iG-CLC) versus chemical looping with oxygen uncoupling (CLOU), Energy Technol. 4 (10) (2016) 1130–1136, https://doi.org/10.1002/ente.201500458.
[23] A. Abad, P. Gayán, R. Pérez-Vega, F. García-Labiano, L.F. de Diego, T. Mendiara, M.T. Izquierdo, J. Adánez, Evaluation of different strategies to improve the efficiency of coal conversion in a 50 kWth chemical looping combustion unit, Fuel 271 (2020), 117514, https://doi.org/10.1016/j.fuel.2020.117514.
[24] C. Linderholm, M. Schmitz, P. Knutsson, M. Källén, A. Lyngfelt, Use of low-volatile solid fuels in a 100 kW chemical-looping combustor, Energy Fuel 28 (9) (2014) 5942–5952, https://doi.org/10.1021/ef501067b.
[25] H. Chen, M. Cheng, L. Liu, Y. Li, X. Li, N. Cai, Coal-fired chemical looping combustion coupled with a high-efficiency annular carbon stripper, Int. J. Greenh. Gas Contr. 93 (2020), 102889, https://doi.org/10.1016/j.ijggc.2019.102889.
[26] I. Gogolev, A.H. Soleimanisalim, C. Linderholm, A. Lyngfelt, Commissioning, performance benchmarking, and investigation of alkali emissions in a 10 kWth solid fuel chemical looping combustion pilot, Fuel 287 (2021), 119530, https://doi.org/10.1016/j.fuel.2020.119530.
[27] J. Yan, L. Shen, S. Jiang, J. Wu, T. Shen, T. Song, Combustion performance of sewage sludge in a novel CLC system with a two-stage fuel reactor, Energy Fuel 31 (11) (2017) 12570–12581, https://doi.org/10.1021/acs.energyfuels.7b02493.
[28] D.C. Guío-Pérez, T. Pröll, H. Hofbauer, Influence of ring-type internals on the solids residence time distribution in the fuel reactor of a dual circulating fluidized bed system for chemical looping combustion, Chem. Eng. Res. Des. 92 (6) (2014) 1107–1118, https://doi.org/10.1016/j.cherd.2013.10.018.
[29] R. Pérez-Vega, A. Abad, J. Bueno, F. García-Labiano, P. Gayán, L. Diego, J. Adánez, Improving the efficiency of chemical looping combustion with coal by using ring-

type internals in the fuel reactor, Fuel 250 (2019) 8–16, https://doi.org/10.1016/j.fuel.2019.03.137.
[30] J.-H. Lim, J.-H. Shin, K. Bae, J.-H. Kim, D.-H. Lee, J.-H. Han, D.-H. Lee, Hydrodynamic characteristics of bubbles in bubbling fluidized bed with internals, Korean J. Chem. Eng. 32 (9) (2015) 1938–1944, https://doi.org/10.1007/s11814-015-0131-x.
[31] J.-X. Zhu, M. Salah, Y. Zhou, Radial and axial voidage distributions in circulating fluidized bed with ring-type internals, J. Chem. Eng. Jpn. 30 (5) (1997) 928–937.
[32] P. Jiang, H. Bi, R. Jean, L. Fan, Baffle effects on performance of catalytic circulating fluidized bed reactor, AICHE J. 37 (9) (1991) 1392–1400, https://doi.org/10.1002/aic.690370911.
[33] C. Zheng, Voidage redistribution by ring internals in fast fluidization, in: Fluidization'91 Science and Technology, 1991, pp. 168–177.
[34] T. Djerf, Solids Flow in Large-Scale Circulating Fluidized Bed Furnaces, Chalmers University of Technology: Gothenburg, Sweden, 2021.
[35] D. Kunii, O. Levenspiel, CHAPTER 4 - the dense bed: distributors, gas jets, and pumping power, in: D. Kunii, O. Levenspiel (Eds.), Fluidization Engineering, Second edition, Butterworth-Heinemann, Boston, 1991, pp. 95–113.
[36] S.B.R. Karri, T.M. Knowlton, 4@ Gas Distributor and Plenum Design in Fluidized Beds, 1998.
[37] Cold Flow Model – Films of Volatiles' Distributor (VD). http://www.entek.chalmers.se/lyngfelt/data/VD_P3.html, 2022.
[38] A. Svensson, F. Johnsson, B. Leckner, Bottom bed regimes in a circulating fluidized bed boiler, Int. J. Multiphase Flow 22 (6) (1996) 1187–1204, https://doi.org/10.1016/0301-9322(96)00025-0.
[39] W. Namkung, S. Done Kim, Gas backmixing in a circulating fluidized bed, Powder Technol. 99 (1) (1998) 70–78, https://doi.org/10.1016/S0032-5910(98)00092-8.
[40] Y. Zhang, C. Lu, J. Grace, X. Bi, M. Shi, Gas back-mixing in a two-dimensional baffled turbulent fluidized bed, Ind. Eng. Chem. Res. 47 (21) (2008) 8484–8491, https://doi.org/10.1021/ie800906n.